From the Department of Physiology and Pharmacology
Karolinska Institutet, Stockholm, Sweden

# APPLICATIONS OF NANOTECHNOLOGY IN NEUROSCIENCE: Functionalized superparamagnetic nanoparticles as contrast enhancers in experimental magnetic resonance imaging

Fu-Hua Wang M.D.


Stockholm 2010

*In Memory of My Grandfather and My Parents*

Published by Karolinska Institutet. Printed by Larserics Digital Print AB


ISBN 978-91-7409-910-2

# ABSTRACT

Magnetic resonance imaging (MRI) is a noninvasive imaging technique that helps clinicians not only to diagnose but also to plan the treatment of invasive surgery and actually treat medical conditions. Superparamagnetic iron oxide nanoparticles (SPIONs) are a family of MRI contrast agents that improves MRI sensitivity/specificity. The aim of this thesis was to caracterize newly developed target specific MRI contrast enhancers using SPIONs. The specific objectives were: Functionalization of SPIONs; Characterization of the functionalized SPIONs with the properties of MR image, biocompatibility and *in vivo* interactions.

Chemical surface modifications of SPIONs were carried out in three ways: (a) by coating polymeric starch, ethanolamine or aminopropyltrimethoxysilane with co-precipitation of magnetite in the matrix of these substances; or (b) by coating gold with coprecipitation of magnetite and subsequent reduction of Au on the surface; or (c) conjugate bovine serum albumin (BSA) to the surface of the particles using the zero-length cross-linker 1-ethyl-3-(3 dimethylaminopropyl) carbodiimde hydrochloride (EDC). A method based on capillaryelectrophoresis with laser-induced fluorescence detection (CE/LIF) was developed to determine the conjugation efficiency of proteins or other primary amino group containing molecules linked to SPIONs.

Monocrystalline iron oxide nanoparticles (MIONs) are a type of SPIONs with an optimal size of 10-30 nm, when starch coated MIONs (Starch-MIONs) were infused into the striatum of the rats, $T_2$*-imaging showed that Starch-MIONs were capable of diffusing in the brain parenchyma. Additional studies showed when Dextran or gold coated MIONs (Dextran-MIONs) or (Au-MIONs) were infused into the striatum of the rats. $T_2$-weighted imaging revealed that increasing the infusion volume resulted in a dramatic expansion of the labeled area of Dextran-MIONs. Similar effects were observed when the infusion dose or retention time was increased. In contrast, Au-MIONs were static at the local injection area and no diffusion was observed. In addition, after two weeks, the signal of Dextran-MIONs was much attenuated whereas Au-MIONs still produced strong signals.

Au-MIONs were incubated with mouse neural stem cells at a dose of 10 μg Fe/ml without a transfection agent, and Dextran-MIONs were used at a dose of 10/100 μg Fe/ml as a control. A 100% labeling efficiency was observed with Au-MIONs 24 hours after incubation, but no uptake was detected for Dextran-MIONs even at a dose of 100 μg Fe.

Green fluorescent protein positive neural stem cells (GFP-NSCs) were labeled with Au-MIONs. Without any transfection agent, an 80% labeling efficiency was observed 24 hours after incubation. The Au-MIONs labeled GFP-NSCs were tested in agar medium and a dose-dependent attenuation of MRI signals was observed for the labeled cells in samples containing as few as only 20 cells. The labeled cells were infused into the spinal cord of rats and tracked by MRI for a period of one month. Histological analysis revealed that MRI correlated well with gold-positive staining of transplanted cells.

In summary, SPIONs can be functionalized with certain substances. The coating efficiency can be monitored by CE/LIF via primary amino groups within the coating substances. Both Starch-MIONs and Dextran-MIONs were capable of diffusing through the interstitial space of brain parenchyma and were progressively cleared out, which can be beneficially used in drug or molecule target delivery and MRI applications for tracing and therapy. Au-MIONs possess superior stability and surface properties, the latter enabling rapid cellular uptake of the particles under physiological conditions. These properties make Au-MIONs especially suitable for tracking transplated cells by MRI.

# LIST OF PAPERS

This thesis is based on the following papers, which will be referred to by their Roman numerals

I. Kim DK, Mikhaylova M, **Wang FH**, Kehr J, Bjelke B, Zhang Y, Tsakalakos T, Muhammed M. Starch-coated superparamagnetic nanoparticles as MR contrast agents. *Chemistry of Materials* 2003; 15:4343-4351.

II. **Wang FH**, Yoshitake T, Kim DK, Muhammed M, Bjelke B, Kehr J. Determination of conjugation efficiency of antibodies and proteins to the superparamagnetic iron oxide nanoparticles by capillary electrophoresis with laser-induced fluorescence detection. *Journal of Nanoparticle Research* 2003; 5:137-146.

III. **Wang FH**, Kim DK, Yoshitake T, Lee IH, Hu XJ, Muhammed M, Bjelke B, Kehr J. Diffusion and Clearance of Superparamagnetic Iron Oxide Nanoparticles Infused into the Rat Striatum Studied by MRI and Histochemical Iron Staining Techniques. Manuscript.

IV. **Wang FH**, Saltó C, Johansson SM, Kim DK, Lee IH, Muhammed M, Arenas E, Bjelke B, Spenger C, Kehr J. Evaluation of gold-coated and dextran-coated iron oxide nanoparticles for labelling neural stem cells. Manuscript.

V. **Wang FH**, Lee HI, Holmström N, Yoshitake T, Kim DK, Muhammed M, Frisén J, Olson L, Spenger C, Kehr J. Magnetic resonance tracking of nanoparticle labelled neural stem cells in a rat´s spinal cord. *Nanotechnology* 2006; 17:1911-1915.

# ABBREVIATIONS

| | |
|---|---|
| aCSF | Artificial cerebrospinal fluid |
| Au-MIONs | Gold-coated monocrystalline iron oxide nanoparticles |
| BSA | Bovine serum albumin |
| CE | Capillary electrophoresis |
| CE/LIF | Capillary electrophoresis with laser-induced fluorescence detection |
| CE/UV | Capillary electrophoresis with ultraviolet detection |
| DAB | Diaminobenzidine |
| Dextran-MIONs | Dextran-coated monocrystalline iron oxide nanoparticles |
| DMEM F12 | Dulbecco's Modified Eagle Medium: Nutrient Mixture F-12 |
| EDC | 1-ethyl-3-(3-dimethylaminopropyl) carbodiimide hydrochloride |
| FID | Free induction decay |
| fMRI | Function MRI |
| GDNF | Glial cell line-derived neurotrophic factor |
| GDNF-NSCs | Neural stem cells with encoded GDNF expression |
| GFAP | Glial fibrillary acidic protein |
| GFP | Green fluorescent protein |
| GFP-NSCs | Neural stem cells with viral transduction of GFP |
| ID | Inside diameter |
| IgG | Immunoglobulin G |
| MIONs | Monocrystalline iron oxide nanoparticles |
| MRI | Magnetic resonance imaging |
| NDA | Naphthyldialdehyde |
| NOS | Nitric oxide synthetase |
| NSCs | Neural stem cells |
| PBS | Phosphate buffered saline |
| RES | reticuloendothelial system |
| RF | Radiofrequency |
| SI | Signal intensity |
| SPIONs | Superparamagnetic iron oxide nanoparticles |
| Starch-SPIONs | Starch coated SPIONs |
| TA | Transfection agents |
| TEM | Transmission electron microscopy |
| TH | Hydroxylase |
| UV/VIS | Ultraviolet /visible spectrometry |
| VIM | Vimentin |

# CONTENTS

# 1 INTRODUCTION

Superparamagnetic iron oxide nanoparticles (SPIONs) are used for a great number of biomedical and clinical applications (1-6). Magnetic resonance imaging (MRI) is a technique most commonly used in medical settings to visualize the internal structure (7-9) and function of the body (10-12). SPIONs are a family of MRI contrast agents that improve MRI sensitivity/specificity (13-15) and opens an important field of research into more specific agents adapted to clinicians needs in the diagnosis and treatment of medical conditions (16-21).

## 1.1 Superparamagnetic iron oxide nanoparticles (SPIONs)

### 1.1.1 Biomedical Applications of SPIONs

SPIONs with appropriate surface chemistry have been used for a great number of biomedical applications including MRI contrast enhancement, drug delivery, hyperthermia, and *in vitro* bioseparation (22-24).

**1.1.1.1 SPIONs as MRI contrast agents:** SPIONs are powerful enhancers of $T_2$ weighted and $T_2$* relaxation times i.e. causing attenuation in the MRI signal intensity (negative contrast effects), which have been used in multiple ways to enhance MRI sensitivity and specificity.

***Passive targeting*:** The basic mechanism of passive targeting is based on the fact that the *in vivo* kinetics of SPIONs is greatly dependent on particle sizes and surface modification, which can be specifically taken up by some of the tissue cells. This difference changes the local proton environment, thereby increasing the contrast between normal and pathological tissues e.g. tumor, inflammation and lesions (25-27). Smaller particles have a longer circulation time and have been used to increase the sensitivity of perfusion imaging e.g. organ perfusion imaging (28, 29), function MRI (fMRI) (30-32) and tumor vascularity perfusion (33, 34).

***Specific targeting*:** SPIONs conjugated with ligands give the particles targeting ability towards specific tissues. Weissleder *et al*. attached SPIONs to antimyosin Fab for

immunospecific MRI of cardiac infarcts resulting in a marked decrease in the signal intensity of infarcted myocardium (35, 36). In another study, when polyclonal IgG was attached to SPIONs, the SPIONs-IgG caused enhancement of MRI at the site of inflammation in an animal model of myositis (37, 38). The recently developed arginine–glycine–aspartic acid (RGD) )-containing peptide coated SPIONs were found to enhance MRI at the site of xenoplanted U87MG tumor cells after intravenous injection (39).

***Labeled cells for imaging*:** SPIONs have been used to label cells *in vitro* and these labeled cells could then be tracked by MRI *in vivo*, which is promising in the recent progress in stem cell and progenitor cell based therapies (40-42). This technique has been performed successfully in animal studies, e.g. Yeh and colleagues demonstrated the MRI tracking of SPIONs labeled rat T-cells in rat testicles with tissue inflammation induced by the local injection of a calcium ionophore to attract T-cells (43). Krieg and colleague used SPIONs-labeled neurophils as inflammation-specific contrast agents for MRI (44). SPIONs-labeled olfactory ensheathing cells have also been successfully tracked by MRI in the rat spinal cord (45). Techniques for cellular labeling include attaching SPIONs to the cell surface (46-48); internalizing biocompatible SPIONs by fluid phase endocytosis (49, 50), receptor-mediated endocytosis (51, 52) or phagocytosis (53, 54). The most commonly used nanoparticles are dextran coated SPIONs. However, dextran coated particles are not presently sufficient for cellular uptake. To offset this disadvantage, one strategy has been to use a transfection agent to substitute the fluid phase endocytosis pathway (41, 55, 56) or to use a receptor-mediated endocytosis pathway by coupling dextran-coated particles with specific ligands (52, 57). The latter is specially advantageous for specific cell labeling.

**1.1.1.2 Active drug targeting:** SPIONs can be used as carriers for the site-specific delivery of drugs since their intrinsic superior magnetic property gives them the ability to respond and aggregate upon the application of an external magnetic field. This feature has been exploited to transport drug loaded SPIONs to areas of interests where the drugs are subsequently released in a controlled manner (58, 59). For these applications, the size, surface charge and surface chemistry of the nanoparticles are particularly important and strongly affect the blood circulation time of the particles within the body (60-62). The internalization of SPIONs is especially dependent on the size of the particles. For intravenous injection, if the diameter of the particles is larger than 200nm, they are usually sequestered by the spleen and are

eventually removed by the cells of the phagocyte system as a result of mechanical filtration resulting in decreased blood circulation times. Small particles with diameters of less than 10 nm are rapidly removed through extravasations and renal clearance. Particles with diameters ranging between 10 and 100 nm are optimal for intravenous injection and have the most prolonged blood circulation times (61, 63). In this case, the particles are small enough to evade the reticuloendothelial system (RES) of the body and capable of penetrating the capillaries of the tissues and offer the most effective distribution in targeted tissues (22, 64).

SPIONs are also actively involved in gene delivery (65, 66). Polyethyleneimine (PEI) coated SPIONs, with the application of an external magnetic field, have greatly enhanced transfection efficiency (22).

**1.1.1.3 Hyperthermia:** Hyperthermia is an experimental treatment for malignant tumors (67, 68). Tumor cells are sensitive to heat because of the states of hypoxia, acidification and poor nutrition, and can be destroyed at temperatures higher than 43 °C whereas normal cells can survive at higher temperatures. Routine heating methods of the entire body include using e.g. hot wax, hot water bath, infrared, radiofrequency, ultrasound and hot blood has been tried as heating therapies for human cancer (69). However, the main problem is that it is less accurate to generate and control heat in tumors than normal tissue. SPION-induced hyperthermia is based on the fact that these particles produce heat during exposure to external alternating current magnetic fields. Surface modified SPIONs of appropriate size can diffuse into tumor tissue and into tumor cells by endocytosis (70, 71). Subsequently, heat can be generated by the magnetic moments oscillates, which converts the electromagnetic energy into heat (67, 68). In addition, during hyperthermia treatment, heating can increase the membrane permeability, which can be beneficial for using hyperthermia in combination with chemotherapy (72, 73).

### 1.1.2 SPIONs synthesis

Iron oxides are used in a general sense to either magnetite ($Fe_3O_4$) or maghemite ($\gamma$-$Fe_2O_3$). Magnetite has the standard formula $A(B)_2O_4$. The A is $Fe^{+2}$ and the B is $Fe^{+3}$. $Fe_3O_4$ is not very stable and is sensitive to oxidation, which can be transformed into $\gamma$-$Fe_2O_3$ in the presence of oxygen. Numerous chemical reactions can be used to synthesize SPIONs. The

classic way is to co-precipitate $Fe^{2+}$ and $Fe^{3+}$ salts in aqueous medium by addition of a base (Equation 1).

$$Fe^{2+} + 2Fe^{3+} \xrightarrow[pH\sim9.0,\ 60°C]{\text{co-precipitation}} \text{SPIONs}$$

Equation 1. Scheme to illustrate the synthesis of SPIONs via co-precipitation.

In order to control the SPIONs´growth and to stabilize the particles from agglomeration, some polymers are added during the precipitation process, which coat the surface of the particles to create electrostatic/static repulsion to balance the attraction forces among the particles (74).

### 1.1.3 Surface modification of SPIONs

Surface coating is of utmost importance in determining the stability of SPIONs under physiological conditions. In the absence of any surface coating, the particles are hydrophobic. Due to hydrophobic interactions and the strong magnetic dipole-dipole interactions, the particles tend to agglomerate (22, 75). For effective stabilization of the particles, various methods have been developed.

***Surface modification with monomeric stabilizers***: Functional groups, including carboxylates, phosphates, and sulfates, are known to bind to the surface of magnetites (76, 77). One such example is citric acid (77). This acid can be adsorbed on the surface of the particles by coordination via one or two the carboxylate functionalities, depending upon steric necessity and the curvature of the surface. This leaves at least one carboxylic acid group exposed to the solvent, which is responsible for making the surface negatively charged and hydrophilic.

***Surface modification with polymeric stabilizers***: Polymeric coatings on magnetic nanoparticles offer a high potential in stabilization and biocompatibility of the particles. The most commonly used polymeric coatings in biomedical applications include dextran, starch and polyethylene glycol (PEG) (78, 79). For example, amphiphilic dextran offers the iron oxide particle hydrophilicity and stability, with the hydrophobic moiety interacting with the inner hydrophobic iron oxide core and the hydrophilic tail sticking out into aqueous solution (80).

***Surface modification with inorganic molecules*:** The most common inorganic material for coating iron oxide particle is silica, but other materials such as gold are also used for coating the particles. These coatings provide not only enhance the stability to the nanoparticles in solution but also help to facilitate the binding of various biological ligands at the nanoparticle surface for various biomedical applications (81, 82).

### 1.1.4 Bioconjugation

In addition to making particles target specific, after modification, various biological substances such as antibodies, proteins, or targeting ligands may also be conjugated to the surface of the modified nanoparticles. These substances have some chemically active groups in their structures such as carboxyl, thiol, or amine, etc., which can react with some active groups on the biovectors to make the particles target specific (83, 84).

### 1.1.5 Magnetic properties of SPIONs

Iron oxide particle materials are classified by their response to an externally applied magnetic field. The ratio of magnetization induced in a magnetic material to the strength of the applied magnetic field is termed magnetic susceptibility. The magnetic susceptibility of superparamagnetic materials is higher than paramagnetic materials, although paramagnetic iron oxides are also used for MRI (85).

The effect of iron oxides on proton relaxation time is described by their relaxivity, i.e. R1 and R2, which change in reverse relaxation time plotted as a function of iron concentration ($mmol/l.s^{-1}$). MR contrast agents´relaxivity is typically measured at 37°C and 0.47T (86). Relaxivity of the contrast agents depends on many variables including the structure and particle size, field strength, medium in which the relaxation times are determined, temperature, etc. Typically R2 values of iron oxides range from 10-1000 ($mmol/l.s^{-1}$). Medium sized (<200 nm) iron oxide particles have been shown to have a higher R2 relaxivity than larger particles. Very small particles on the other hand (<10nm) have a lower R2 (87). Monocrystalline iron oxide nanoparticles (MIONs) are a type of SPIONs with an optimal size of 10-30 nm (35, 88), which were used in the studies presented in this thesis.

The effect of iron oxides on MR signal intensity is best explained by two mechanisms. First, strong magnetic fields introduced in iron oxide particles in a magnetic field shorten the spin relaxation process of nearby protons. Second, there exists a large susceptibility difference between particles and the surrounding medium. It has been shown that diffusion in these field gradients leads to an irreversible loss of phase coherence and thus decreased transverse relaxation times of protons. Because of the decreased $T_2$ relaxation times, tissues containing iron oxides appear hypointense (dark) relative to surrounding tissues on MRI. This effect is most marked on $T_2$ weighted images, especially on T2* images (86).

## 1.2 Magnetic materials and magnetic resonance imaging (MRI)

### 1.2.1 Magnetic properties of materials

***Magnetic field and magnetic induction***: Atoms consist of three fundamental particles: protons, which possess a positive charge; neutrons, which have no charge; and electrons, which have a negative charge. The nucleus of an atom consists of all the protons and neutrons whilst the electrons are located in orbitals surrounding the nucleus. A property of the nucleus is spin. The nucleus can be considered to be constantly rotating around an axis at a constant rate. This self-rotation axis is perpendicular to the direction of rotation (Figure 1). Concurrent with the spinning, a charged nucleus produces a magnetic field, which is oriented parallel to the axis of rotation. This arrangement is analogous to a bar magnet in which the magnetic field is considered to be oriented from the South to the North Pole (Figure 1).

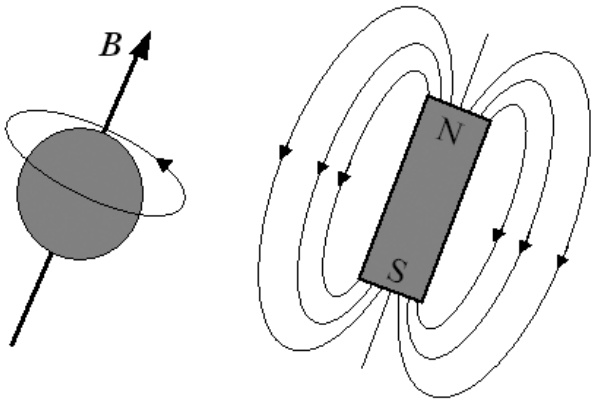


Figure 1. A rotating nucleus with protons produces a magnetic field oriented parallel to the axis of rotation.

Magnetic field strengths are measured in units of gauss (G) and tesla (T). One Tesla is equal to 10,000 gauss.

***Magnetic moment and magnetization***: With the spinning, the nucleus produces a local magnetic field which possesses a magnetic moment. The magnetization of a material is the magnetic moment per unit volume. The magnetic moment ($m$) and magnetization ($M$) measure how a nucleus responds to an applied magnetic field ($B_0$). The relationship between magnetic moment $m$ and magnetization $M$ is given by:

$$M = mB_0 \qquad \text{(Equation 2)}$$

### 1.2.2 Types of magnetic materials

According to the magnetic properties, the materials contain spins that are classified as ferromagnetic, paramagnetic, superparamagnetic and diamagnetic.

***Ferromagnetic materials***: Ferromagnetic materials have a large positive magnetic susceptibility. These materials contain spins that are aligned parallel to each other due to strong positive exchange interaction between the spins, which may have a resultant magnetic moment if there is no applied magnetic field. When ferromagnetic materials are placed in a magnetic field, the field strength is much stronger inside the material than outside. Ferromagnetic materials have the ability to remain magnetized when an external magnetic field is removed. On MR images, ferromagnetic materials cause susceptibility artifacts

characterized by loss of signal and spatial distortion. Generally, ferromagnetic materials contain iron, nickel or cobalt.

***Paramagnetic materials***: Paramagnetic materials have unpaired electrons whose spins are free to change direction, resulting in a positive magnetic susceptibility. When these materials are placed in a magnetic field, the field strength is stronger inside the material than outside but the magnitude of this susceptibility is less than one thousand of that of ferromagnetic materials. Paramagnetic materials do not have an inherent magnetic moment in the absence of an applied field. On MR images, paramagnetic materials increase the $T_1$ and $T_2$ relaxation rates (decrease in the $T_1$ and $T_2$ times). The paramagnetic materials Gd and ferric ion are used as MR contrast agents. At low concentrations, Gd and ferric ion cause preferential $T_1$ shortening, resulting in high intensity on $T_1$ weighted images. At high concentrations, $T_2$ shortening causes a decreased signal intensity.

***Superparamagnetic materials***: Superparamagnetic materials consist of two spin lattices pointing in opposite directions and the number of spins on each lattice may have different populations leading to a net magnetic moment. Their magnetic susceptibility is between that of ferromagnetic and paramagnetic materials. On MR images, superparamagnetic materials cause the marked shortening **of** both $T_1$ and $T_2$ relaxation time resulting in loss of signal in all commonly used pulse sequences. This results in high intensity decrease in $T_2$ weighted images and the efficiency is larger than paramagnetic materials (86). The superparamagnetic iron oxide, Magnetite ($Fe_3O_4$), is commonly used and developed as a strong MR contrast agent.

***Diamagnetic materials***: Diamagnetic materials consist of two spin lattices pointing in opposite directions and the number of spins on each lattice have similar populations, which giving a negligible net magnetic moment. When these materials are placed in a magnetic field, they weakly repel the field resulting in a small negative magnetic susceptibility. Diamagnetic materials include water, copper and most tissues.

### 1.2.3 Nuclear magnetic resonance and MRI

**1.2.3.1 Magnetization**: Nuclei possess a property known as nuclear spin. Consider an arbitrary volume of material containing protons located outside a magnetic field. Each proton has a spin vector of equal magnitude. However, the spin vectors for the entire collection of protons within the tissue are randomly oriented in all directions. Performing a vector addition of these spin vectors produces a zero sum: no net magnetization is observed in the tissue (Figure 2).

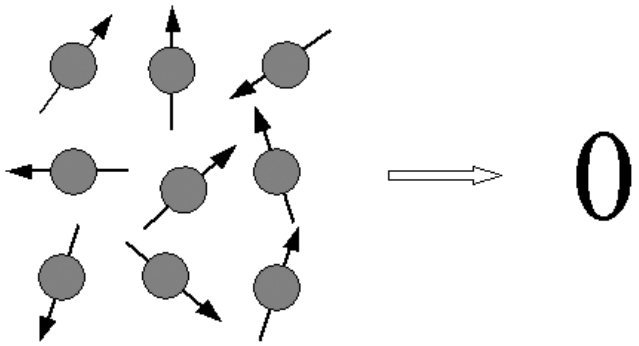


Figure 2. In the absence of a magnetic field, the protons have their spin vectors oriented randomly and the vector sum of these spin vectors is zero.

If the material is placed inside a magnetic field $B_0$, the individual protons begin to rotate (precess) about the magnetic field. The protons are tilted slightly away from the axis of the magnetic field, but the axis of rotation is parallel to $B_0$. This precession occurs because of the interaction of the magnetic field with the moving positive charge of the nucleus. By convention, $B_0$ is defined to be oriented in the $z$ direction of a Cartesian coordinate system; the axis of precession is also the $z$ axis. The motion of each proton can be described by a unique set of $x$, $y$ and $z$ coordinates. The perpendicular, or transverse, coordinates are nonzero and vary with time as the proton precesses, but the $z$ coordinate is constant with time (Figure 3).

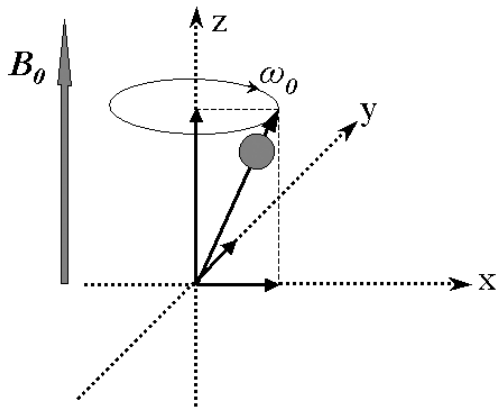


Figure 3 Inside a magnetic field, a proton precesses about the magnetic field.

The rate or frequency of precession is proportional to the strength of the magnetic field and is expressed by the Larmor equation:

$$\omega_0 = \gamma B_0 / 2\pi \qquad \text{(Equation 3)}$$

where $\omega_0$ is the Larmor frequency in megahertz (MHz), $B_0$ is the magnetic field strength in Tesla (T) that the proton experiences, and $\gamma$ is a constant for each nucleus in $s^{-1}$ $T^{-1}$, know as the gyromagnetic ratio, which is different for different nuclei.

The spins can be either parallel (low energy level) or anti-parallel (high energy level) to the magnetic field $B_0$. The number of protons in the lower energy level is greater than the number in the higher level, leading to a net magnetization that is different from zero (Figure 4).

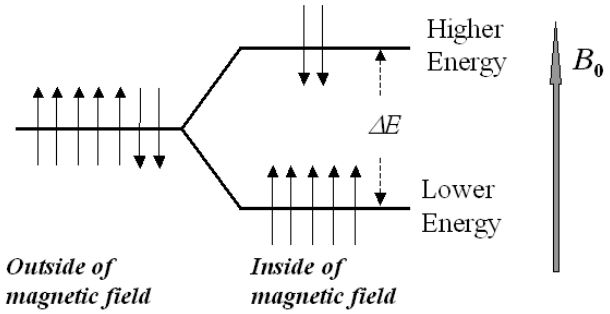


Figure 4. Zeeman splitting for protons.

The amount of protons in each level is governed by the Boltzmann distribution:

$$N_{upper} / N_{lower} = e^{-\Delta E/kT} \qquad \text{(Equation 4)}$$

Where $N_{upper}$ and $N_{lower}$ are the number of protons in the upper and lower energy levels, ΔE is the energy difference between the two levels, $k$ is Boltzmann´s constant ($1.381 \times 10^{-23} JK^{-1}$), and T is the absolute temperature (K). Since ΔE depends on the field strength $B_0$, the exact number of spins in each level also depends on $B_0$ and increase with increasing $B_0$. This unequal number of protons in each energy level means that the vector sum of spins, known as the net magnetization ($M_0$) will be nonzero and will point parallel to the magnetic field $B_0$ (figure 5). The direction of the magnetic field has been defined as the z-direction of $M_0$. The components of $M_0$ in the x- and y-direction are zero. If there is absorption of energy, more protons will become antialigned, but when the energy supply is stopped, the protons will always strive to return to equilibrium. Larger field strength $B_0$ means a greater value of $M_0$, resulting in a more intense MR signal. This induced magnetization $M_0$ is the source of signal for MR experiments.

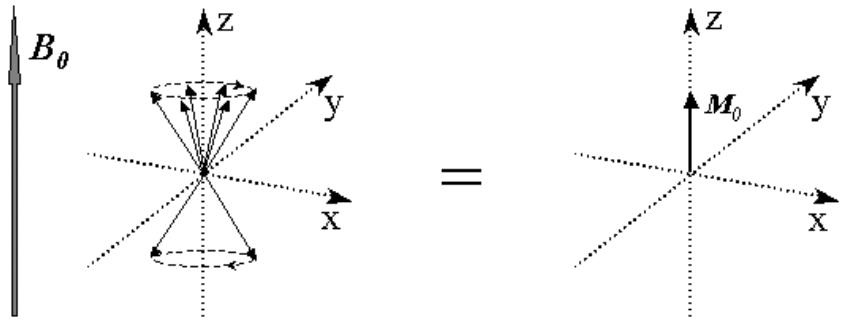


Figure 5. Alignment of the individual magnetic moments with an external magnetic field.

**1.2.3.2 Excitation**: Given a radio frequency (RF) pulse onto the material with a frequency equal to the precession of the spins, the spins will be excited from the lower energy orientation to the higher energy orientation. At the same time, a spin in the higher energy level will be stimulated to release its energy and will go to the lower energy level. Because there are more spins in the lower energy state, there is a net absorption of energy by the spins in the material. This quantized energy absorption is known as resonance absorption and the

frequency of energy is known as the resonant frequency. The RF pulse causes a magnetic field $B_1$ (Figure 6).

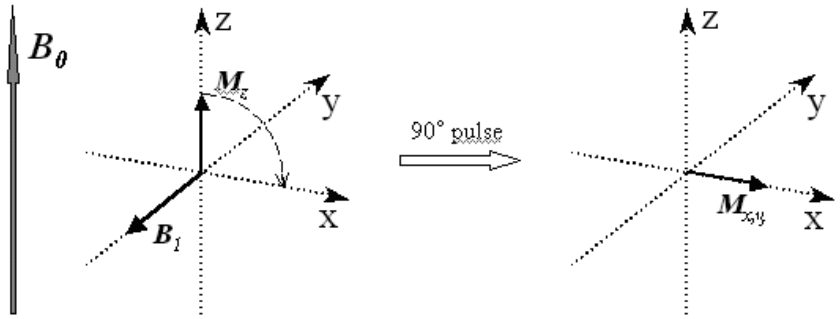


Figure 6. Effect of a 90º RF pulse.

$B_1$ interacts with the magnetization and makes the magnetization vector $M_0$ ($M_z$, $M_{x,y}$) rotate around the $B_1$ field. The change in the procession angle of the net magnetization vector is dependent on the length and amplitude of the RF pulse. If the RF pulse is powerful enough to flip $M_0$ down by 90° it is called a 90° pulse (Figure 6). If the pulse flipped $M_0$ down by 180° it is called a 180° pulse and so on. Strong RF pulse means high $B_1$ field and more flip angle of $M_0$, high $B_0$ field means high basic frequency. .

**1.2.3.3 Relaxation**: After the application RF pulse the protons release the absorbed energy and return to their original configuration i.e. the magnetization $M_0$ decays back to the equilibrium state. There are two major processes contributing to the return of $M_0$ to the equilibrium state: $T_1$ relaxation and $T_2$ relaxation. The relaxation is characterized by relaxation times, $T_1$ and $T_2$.

***$T_1$ relaxation***: The return of excited nuclei from the high energy state to the low energy is associated with loss of energy to the surrounding nuclei. $T_1$ relaxation is characterized by the longitudinal return of the net magnetization to its ground state of maximum length in the direction of the main magnetic field (along the *z* axis). $T_1$ relaxation is also called spin-lattice relaxation, the spins in the high energy state release their energy to the surrounding lattice. The relaxation time $T_1$ is the time required for the *z* component of $M_0$ to return to 63% of its original value following a 90° RF pulse. This return of magnetization follows the equation:

$$M_z = M_0(1\text{-}e^{-t/T1}) \qquad \text{(Equation 5)}$$

where t is the time following the RF pulse. After 3 $T_1$ times, $M_0$ is at 95 % of its original length. Spins are usually considered completely relaxed after 5 $T_1$ times. $T_1$ relaxation is dependent on the main magnetic field strength that specifies the Larmor frequency. When the frequency of the rotations is close to or at the Larmor frequency, $T_1$ relaxation is fastest.

***$T_2$ relaxation***: $T_2$ relaxation is also called spin-spin relaxation. The spins in the high and low energy state exchange energy but do not loose energy to the surrounding lattice. This results in loss of the transverse magnetization (in the *xy* plane). The $T_2$ relaxation time is the time required to decay 63% of the transverse magnetization after a 90° RF pulse. This return of magnetization follows the equation:

$$M_{xy} = M_0e^{-t/T2} \qquad \text{(Equation 6)}$$

$T_2$ is less than or equal to $T_1$, e.g. in pure water $T_2$ is approximately the same as $T_1$, but in biological materials, $T_2$ is considerably shorter than $T_1$.

***$T_2$* relaxation***: $T_2$* relaxation is the loss of signal seen with dephasing of individual magnetizations. It is characterized macroscopically by loss of transverse magnetization at a rate greater than $T_2$. It is caused by magnetic field inhomogeneity and occurs in all magnets. The relationship between the $T_2$ from molecular processes and that from inhomogeneities in the magnetic field is as follows.

$$1/T_2\text{*} = 1/T_2 + 1/T_{2\ \text{inhomo}}. \qquad \text{(Equation 7)}$$

Therefore, gradient echo sequences are more susceptible to ferromagnetic foreign bodies that distort the main magnetic field homogeneity.

**1.2.3.4 Free induction decay**: As mention above, after an RF pulse the protons immediately release the absorbed energy and return to their original equilibrium orientation. If a coil is placed perpendicular to the xy plane, the protons induce a voltage in the coil during their precession. This voltage decays with time through the relaxation. This is the MR signal, called free induction decay (FID) (Figure 7).

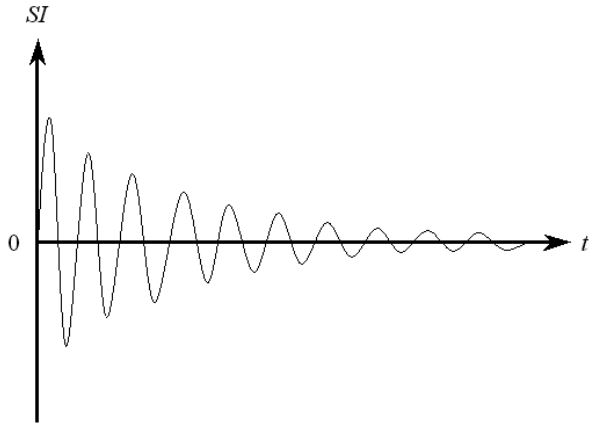


Figure 7. Free induction decay (FID).

Where *SI* is signal intensity.

**1.2.3.5 Basic measurement of $T_1$ relaxation using the inversion-recovery pulse sequence**: $T_1$ can be measured using a 180°-τ-90º pulse sequence. A 180° pulse is applied. $M_0$ rotates down parallel to the *z* axis in the negative direction. After a time τ a 90º pulse is applied to push $M_0$ into the *xy* plane to make a detectable FID signal.

**1.2.3.6 Basic measurement of $T_2$ relaxation using the spin-echo pulse sequence**: $T_2$ can be measured using a 90º τ-180° pulse sequence. First a 90° pulse rotates $M_0$ down in the *xy* plane, then a 180° pulse is applied to rotate spins around in the *xy* plane, during the rephrasing a free induction `echo´ signal is detected.

# 2 AIMS

**General aim**:

To caracterize target specific MRI contrast enhancers based on SPIONs using MRI and immunohistochemistry concerning biocompatibility testing *in vitro* and *in vivo* and *in vivo* documentation of distribution and elimination.

**Specific aims**:

- To caracterize; surface modification and bioconjugation combined with establishing a high sensitivity method to determine the conjugation efficiency of antibodies or other primary amino group containing molecules to SPIONs.

- To caracterize; the properties of SPIONs with different surface modifications using MRI.

- To caracterize; the capacity of diffusion and clearance of the surface modified SPIONs in the rat striatum and their biocompatibilities with the brain tissue.

- To caracterize; the potential of surface chemisorption of gold coated SPIONs in cells by adhesion or endocytosis as a tool for labelling stem cells.

- To evaluate; gold coated SPIONs as a cell label for tracking transplanted stem cells *in vivo*.

# 3 MATERIALS AND METHODS

## 3.1 SPIONs

### 3.1.1 Synthesis and surface modification

***Starch coated MIONs (Stach*-MIONs):** Aqueous dispersion of MIONs was achieved by alkalinizing an aqueous mixture of ferric and ferrous salts with NaOH at room temperature. $N_2$ gas was bubbled through the reaction medium during synthesis in a closed system. The detailed procedure of this controlled co-precipitation approach has been reported (89, 90). A specific amount of the Fe stock solutions was poured into a prepared starch solution under vigorous stirring. A 25 ml portion of the starch and iron mixture was then added drop-wise into 200 ml of 1.0 M NaOH under vigorous mechanical stirring (2000 rpm) at 60 °C for 2 hours. After the starch was completely dissolved, the solution was quickly placed in a 60 °C water bath. The gels formed were washed with deionized water until the pH became less than 8.5. During the boiling, around 50 % of the water was evaporated and the remaining solution was cooled to room temperature and kept for 12 hours. The Starch-MIONs were dialyzed for the removal of excess unreacted starch at 37 °C for 2-3 days while being continuously stirred.

***Ethanolamine/aminopropyltrimwthoxysilane coated SPIONs***: SPIONs were synthesized using the chemical co-precipitation method as described above. However, the particles were coated with entanolamine (hydrodynamic diameter of 107 nm)/aminopropyltrimethoxysilane (hydrodynamic diameter of 183 nm) directly during the coprecipitation reaction (90).

***Gold coated MIONs (Au-MIONs)***: Au-MIONs (mean hydrodynamic diameter of 20 nm) were synthesized using a water-in-oil reverse microemulsion ($\mu E$) system by coprecipitation of magnetite and subsequent reduction of gold on the surface of the magnetite using $NaBH_4$, as described elsewhere (91).

***Dextran coated MIONs (Dextran-MIONs)***: Dextran-MIONs (hydrodynamic diameter of 20 nm) were purchased from Dr Weissleder´s laboratory (Harvard Medical School, MA, USA),

with a suspension containing 11.92 mg Fe/ml of 0.025 M sodium citrate, were diluted in artificial cerebrospinal fluid (aCSF) for intracerebral inoculation.

***Bioconjugation of SPIONs*:** MIONs were conjugated with bovine serum albumin (BSA) using the zero-length cross-liker 1-ethyl-3-(3-dimethylaminopropyl) carbodiimide hydrochloride (EDC). Briefly, the iron oxide particles (0.6 mg/ml) were resuspended three times in the phosphate buffer (0.1 M, pH 6.3) using the ultrasound bath for 2 min. EDC and BSA (each at the concentration of 0.6 mg/0.5 ml) were dissolved in the phosphate buffer and kept at 4 ºC. To this solution, 1 ml of the nanoparticles was added and the whole reaction mixture was incubated under constant shaking for 24 hours. Finally, the particles were repeatedly purified from the unreacted BSA by magneto-extraction, i.e. a strong external magnet was used to retain the magnetic material inside the vial the reaction mixture was discarded and replaced with the phosphate buffer (SPB).

### 3.1.2 Characterization

Spectrophotometric determination of the iron content in the diluted samples was performed by ferrozine method as follows: the iron oxide nanoparticles were dissolved in 12 M hydrochloric acid to form $Fe^{+3}$ and $Fe^{+2}$ ions. The solution was mixed with the ferrozine reagent (Hach, Chicago, Illinois, USA) and absorbance of the resulting complex was measured at the wavelength of 562nm.

***Transmission electron microscopy (TEM) measurement*:** A TEM study was carried out on a JEOL-2000EX microscope with an electron kinetic energy of 200 kV. The specimen for TEM imaging was prepared from the SPIONs suspension in deionized water using sonication for 3 min. After sonication, 1 ml of the SPIONs suspension was centrifuged for 5 min at 14000 rpm. A drop of well dispersed supernatant was placed on a carbon-coated 200 mesh copper grid, followed by drying the sample at ambient conditions before it was attached to the sample holder on the microscope. The particle size and size distribution were calculated from TEM images for all prepared samples using an image analysis program by measuring the diameters of at least 500 particles.

***ξ-potential measurement*:** The ξ-potential of the SPIONs suspension was measured in $5x10^{-3}$ and $1x10^{-2}$ M NaCl background electrolyte solutions using a Zetasizer 2000. The test suspension was prepared at a fixed concentration in several buffers adjusted to requested pH using NaOH or HCl stock solutions.

***Surface-characterization of SPIONs by using CE/UV***: A Beckman P/ACE capillary electrophoresis (CE) system equipped with filter-based ultraviolet (UV) /visible spectrometry (VIS) detector operating at wavelengths of 200, 214, 254 and 280 nm, respectively, was used. CE separation was carried out using a fused-silica capillary with inside diameter (ID) of 75 μm and the total length of 65 cm (effective length 48 cm). 12.5 mM sodium borate buffer (pH 9.2) was used as a separation buffer. The capillary was sequentially flushed with 1, 0.2 M sodium hydroxide, water and separation buffer (10 min for each) prior to use. The samples were injected by pressure at 50 mbar for 5 sec. A potential of 30 kV was applied and the temperature of the capillary was maintained at 26°C.

***Effect of surface modifications of SPIONs on MR image*:** SPIONs were tested in colloidal suspension. Au-MIONs and Dextran-MIONs were prepared at the concentrations of 1, 3, 10, 30 and 100 ng/μl of Fe in a water medium, and tested by MRI with $T_2$ weighted spin-echo imaging.

### 3.1.3 Determination of coating efficacy of functionalized SPIONs

The protein content of the functionalized nanoparticles was estimated spectrophotometrically at the wavelength of 562 nm and by using the BCA Protein Assay Reagent kit (Pierce, Rockford, Illinos, USA). The amount of protein entrapped within the nanoparticles is calculated as the difference between the total amount used to prepare the nanoparticles and the amount of protein in the unreacted fraction. The functionalized nanoparticles were derivatized with naphthyldialdehyde (NDA)/cyanide reagent as follows: 80 μl of 0.1 M perchloric acid solution, 240 μl of sodium cyanide solution in borate buffer and 40 μl of 5 mM NDA solution were added to 720 μl of sample in separation buffer. The reaction time was 5 min at room temperature. After derivatization, the samples were placed into the sampler of the P/ACE electrophoresis instrument and separated by capillary electrophoresis

with a laser-induced fluorescence detection (CE/LIF) at the wavelengths of 442 nm (excitation) and 488 nm (emission). The laser-induced fluorescence detector ZETALIF was connected to a helium-cadmium laser (22 mW). The separations were carried out using a fused-silica capillary (effective length 48 cm, ID 75 μm) and 100 mM sodium borate buffer (pH 9.2), the samples were injected by pressure at 50 mbar for 2 sec. A potential of 30 kV was applied and the temperature of the capillary was maintained at 26°C.

## 3.2 Cell culture and labeling

***Neural stem cells with encoded GDNF expression*:** Primary neural stem cell lines were generated from neonatal mouse cerebellum (external germinal layer), which produce glial cell line-derived neurotrophic factor (GDNF) as described elsewhere (92, 93). These stem cells were incubated with Au-MIONs at a dose of 10 μg Fe/ml or Dextran-MIONs at a dose of 10-100 μg Fe/ml for 24 hours without the transfection agent (TA). The control group was added with saline only. The cell density during incubation was approximately $2.4 \times 10^4$ per ml medium and 1.77 $cm^2$ growth surface area. Cytospins were fixed with 4% glutaraldehyde, washed, incubated for 5 min with Perl´s solution, washed, and enhanced with 0.5% diaminobenzidine (DAB) (containing 0.15 % hydrogen peroxide).

***Neural stem cells with viral transduction of GFP (GFP-NSCs)*:** Neural stem cells (NSCs) were prepared from the spinal cord of adult female Sprague-Dawley rats (Scanbur BK, Sollentuna, Sweden) as previously described (94). After removal of the meninges, spinal cord tissue was dissociated at 37 °C for 30 min in a solution of 0.7 mg hyaluronic acid, 200 U Dnase and 1.33 mg trypsin per ml. After filtration (70 μm mesh) and centrifugation (200g for 5 min), cells were resuspended in 0.5 M sucrose in 0.5x Hank´s balanced salt solution. After a second centrifugation (750g for 10 min), the cell pellet was resuspended in neurosphere culture medium based on Dulbecco's Modified Eagle Medium: Nutrient Mixture F-12 (DMEM F12, Invitrogen, Carlsbad, CA, USA) with Glutamax and supplemented with 20 ng epidermal growth factor, 20 ng basic fibroblast growth factor, 20 μl B27, 100 U penicillin and 100 μg streptomycin per ml. Neurospheres that had formed after 7 days were dissociated in 1.33 mg/ml of trypsin and single cells were further cultured for 3 days into secondary neurospheres in 50% neurosphere-conditioned medium and 50% fresh medium.

To encode green fluorescent protein (GFP) transduction and label the cells with paramagnetic particles, vesicular stomatitis virus G protein-pseudotyped retroviral particles were prepared (95). Secondary neurospheres were infected 24 hours after passage at a multiplicity of infection of 3.5. The efficiency of the transduction protocol is approximately 60%. Cells were propagated in complete neurosphere culture medium for another 6 hours, thereafter the cells were incubated in 2 ml neurosphere culture medium in the absence or presence of TA TransFast (1 μg/μl, 1 hour at 37 °C) containing Au-MIONs at concentrations of 0.5, 2, 10 and 20 μg Fe/ ml at 37 °C for 24 hours or 48 hours, washed three times with Hank´s balanced salt solution, and harvested with 0.25% trypsin. The cells were counted, and diluted into 1334 cells/μl suspensions in DMEM/Ham´s/F-12 for transplantation.

## 3.3 Animals and surgery

All animal experiments were approved by the local ethical committee (Stockholms Norra djurförsöksetiska nämnd) following the directives of the "Principles of Laboratory Animal Care" (NIH publication No. 85-23) and the Council of the European Communities (86/809/EEC). N 3/00, Börje Bjelke and N91/02, Christian Spenger.

***Infusion of nanoparticles in the rat brain*:** Adult male Sprague-Dawley rats (body weight 250-300 g, delivered by B&K Universal, Sollentuna, Sweden) were anesthetized by sodium pentobarbital (60 mg/kg i.p.). Body temperature was maintained at 36-37ºC using a thermostat regulated heat pad (CMA/105, CMA/Microdialysis, Stockholm, Sweden). The animals were placed in a stereotaxic frame with the incisor bar in –3.2 mm in order to achieve a flat skull position. After the scalp was incised (1.5 mm), the skull was cleaned and a drill hole for microinjection was made (diameter 0.7 mm) using a fine trephine drill, a glass capillary injection cannula (outside diameter of 120 μm) was implanted in the striatum at the coordinates AP + 0.2, L ± 3.1, V – 0.5 mm (from the brain surface). The infusion was performed using a micro infusion pump (CMA/100, CMA/Microdialysis, Stockholm, Sweden) and Hamilton syringe (25 μl). The colloidal nanoparticles were suspended in aCSF at certain concentrations. The colloidal suspensions were infused into the rat striatum at a constant flow rate of 0.5 μl/min. The control rats were injected with aCSF only. After infusion, the injection cannula was withdrawn over a 10 min period and the skin was closed in a single layer.

***Cell transplantation in spinal cord***: Adult male Sprague-Dawley rats (body weight 250-300 g) were anaesthetized with sodium pentobarbital (60 mg/kg i.p.). Body temperature was maintained at 37ºC using a thermostat regulated heat pad (CMA/105, CMA/Microdialysis, Stockholm, Sweden). After laminectomy of T8, the dura was incised, a total of 2 µl Au-MIONs labelled GFP-NSC (0.5 µl at four depths of 1.75, 1.25, 1 and 0.5 mm from the spinal cord surface) was grafted at the midline of the spinal cord. The cell suspension was infused with a 10 µl Hamilton syringe connected to a glass capillary (outer diameter 100 µm) at a speed of 0.5 µl/min (micro infusion pump, CMA/100, CMA/Microdialysis, Stockholm, Sweden). Control animals received Au-MIONs (2 µg Fe/µl) alone, or Dextran-MIONs (2 µg Fe/µl) or aCSF injection.

## 3.4 MRI

***Brain MRI*:** The rats were anaesthetized with isoflurane (5 % for induction and 1.5-2 % for continuous anesthesia, driven by air). The body temperature was maintained within the range of 36-37ºC using a regulated warm air stream. MRI was performed using a 4.7 T, 40 cm diameter horizontal bore (Bruker Biospec Avance 47/40, Bruker, Karlsruhe, Germany) fitted with a 12 cm inner diameter self-shielded gradient system (200 mT/m). A 35 mm volume RF coil was used for signal detection. The main sequence employed was a Bruker implementation of rapid acquisition with relaxation enhancement (RARE) imaging (96). The following MR parameters were used: repetition time (TR) = 2000 ms, echo time (TE) = 46.2 ms, number of averages (NEX) = 8, RARE factor = 16, field of view (FOV) = 4 × 4 cm, matrix dimension = 256 × 256, slice thickness = 0.8 mm.

***Spinal cord MRI*:** A commercially available 1H/31P 40 mm surface coil (Bruker, Karlsruhe, Germany) was used for excitation and signal detection. Animals were anaesthetized with 1.5-2.0 % isoflurane using a facemask adapted to the mouthpiece of the rig. Body temperature was maintained at 36-37 °C using a temperature controlled air stream. $T_2$-weighted 2D spin-echo images were produced with RARE. The following parameters were used: TR = 3000 ms, TE = 21 ms, RARE factor = 8, NEX = 8, FOV = 3.5 × 3.5 cm, matrix dimension = 512 × 512, slice thickness = 1 mm.

***Au-MIONs labeled GFP-NSCs*:** To test the detection limit of MRI for Au-MIONs labeled GFP-NSCs, 1 µl suspensions of GFP-NSC were injected into 0.3% agar (agar / water) with different concentrations (20, 60, 200 cells / µl). Unlabeled GFP-NSCs with the concentration of 200 cells / µl were injected as a control. The MRI protocol is the same as `Brain MRI´ above.

## 3.5 Histology

***Histochemical iron staining*:** Rats were sacrificed immediately by overdose with sodium pentobarbital at certain time intervals after the particles infusion. Brains were removed and fixed by submersion in 10 % neutral buffered formalin for lest 24 hours at room temperature. After fixation, the brains were serially sectioned at 100 µm (coronal) on a microtome (MICROM HM500M, Germany). The free floating sections were subjected into Perl´s solution (equal parts of 2 % HCl and 2 % potassium ferrocyanide) for 30 min at room temperature, rinsed in deionized water for 30 min and incubated in 0.5 % diaminobenzidine (DAB, in 50 mM Tris buffer, containing 0.15 % hydrogen peroxide, pH 7.4) for 30 minutes (97). This stain yields a brown reaction product. The same staining process was carried out for spinal cord iron staining.

For staining cells, the cells in cell cultural dish were fixed with 4% glutaraldehyde, washed, incubated for 5 min with Perl´s solution, washed, and enhanced with 0.5% DAB (containing 0.15 % hydrogen peroxide).

***Histochemical gold staining*:** For the gold staining, a silver enhancement stain was used. Slides were developed in the silver enhancer solutions (Silver enhancer kit; Sigma, St. Louis, MI, USA) at room temperature for approximately 10 min, washed, and fixed by immersion in 2.5% aqueous sodium thiosulfate for 3 min.

***Immunohistochemistry*:** Rats were perfused with 150 ml of 0.9 % saline (contain 10 U/ml of heparin), followed by 150 ml of 4% paraformaldehyde in 0.1M ice-cold phosphate buffer, pH 7.4. The spinal cords were dissected, post-fixed for 1 hour at room temperature, and kept in 10% sucrose for 48 hours at 4˚C. A 2 cm long spinal segment centered at the injection site was longitudinally sectioned at 14 µm thickness on a cryostat. For immunohistochemistry,

the sections were incubated with primary antibodies at 4˚C overnight. Antisera raised in rabbit against GFP (1:200; Molecular probes, Eugene, OR, USA) and in mouse against ED1 (1:200; Serotec,Oxford, UK) were used in 0.3 % Triton X, 0.1 M PBS. After rinsing three times, the sections were incubated with secondary antibodies conjugated with Cy2 or Cy3 (Jackson ImmunoResearch, West Grove, PA, USA) for 1 hour at room temperature. The slides were rinsed again, mounted with anti-fading agent and cover slips for analysis with confocal microscopy (LSM 510 META; Carl Zeiss, Germany).

***Assessment of Tissue Toxicity*:** Adult male Sprague-Dawley rats (body weight 230-250 g) were infused with Au-MIONs or Dextran-MIONs at a dose of 0.1 or 1.0 µg Fe in 0.5 µl aCSF or 0.5 µl aCSF only (control) into the striatum (see *Animals and infusion*). 1 week after inoculation, the rats were anesthetized with sodium pentobarbital (80 mg/kg i.p.) and perfused via the aorta, first with 150 ml of 0.9 % saline (contain 10 U/ml of heparin), followed by 150 ml of Lana´s fixative (98) at room temperature. The rat brains were removed and postfixed in the same fixative for 1 hour, then transferred to 10 % sucrose-phosphate buffered (SPB) and stored at 4°C. The perfused brains were rapidly frozen in gaseous $CO_2$ and sectioned by microtome (MICROM HM500M, Germany); the 14µm cryosections were thawed onto gelatin-coated slides. Sections were rinsed for 3 x 10 min in 0.1M phosphate buffered saline (PBS) before being incubated with primary antibodies diluted in PBS containing 0.3% Triton X-100 for 48 hours in 4°C in a humid chamber. After rinsing for 3 x 10 min in PBS, the slides were incubated in either ALEXA454 or ALEXA594 conjugated secondary antibodies (Molecular probes, diluted 1:500 in 0.3% Triton X-100) for 1 hour at room temperature. After additional rinsing for 3 x 10 min in PBS, the slides were mounted in 90% glycerine in PBS. The primary antibodies used were raised against tyrosine hydroxylase (TH, Diasorin, mouse anti-rat diluted 1:5000) to label dopaminergic neurons, glial fibrillary acidic protein (GFAP, Sigma, mouse anti-human, diluted 1:100), S100 (Dako patts, rabbit anti-cow, diluted 1:300), and vimentin (VIM, Sigma, mouse anti-pig, diluted 1:100) to label astrocytes, OX-42 (Serotec, mouse anti-rat CD11b, diluted 1:100) to label microglia, and nitric oxide synthase (NOS, Chemicon, rabbit anti-rat, diluted 1:100) to visualize the inflammatory reaction. The sections were evaluated using a fluorescent microscope connected to a camera and computer with AxioVision software.

# 4 RESULTS AND DISCUSSION

## 4.1 Functionalization of SPIONs (*Paper I, II, IV, V*)

### 4.1.1 Characterization of SPIONs

***TEM***: TEM image of dried magnetic nanoparticles taken from the corresponding colloidal particles prepared at room temperature. Typically, spherical shapes were formed. A roughly spherical or ellipsoidal shaped particle with some irregularities has the characteristic crystalline order of magnetite and a diameter around 5.7 nm. However, when stored in the solution the hydrodynamic diameter of magnetite nanoparticles measured by light-scattering method was 154 nm at the iron concentration of 769 μg/ml.

***CE-UV***: A sample of these `naked´ SPIONs was introduced into the separation capillary of the CE system and analysed with UV detection at the wavelength of 200 nm. Figure 8A shows the baseline separation of the SPIONs (migration time of 2.08 min) from the neutral marker mesityl oxide (1.47 min). The samples were introduced into the capillary at the anode and they were transported to the cathode by a combination of electroosmosis and electrophoresis (99, 100). The retention of the neutral marker is affected only by the electroosmotic flow, whereas the peak of the later eluting nanoparticles indicates that they moved more slowly, either because of their size or due to their negatively charged surface. This behaviour of the charged particles is in good agreement with the ξ-potential values measured in buffers at different pH (Figure 8B). Thus, the ξ-potential of the uncoated SPIONs at pH 9.2 was –30 mV, which confirms the CE measurement suggesting that the surface of the SPIONs is hydrated and contains negatively charged hydroxyl groups. These hydroxyl groups make it possible to use carbodiimide as a cross-linker of nanoparticles and primary amino group containing molecules.

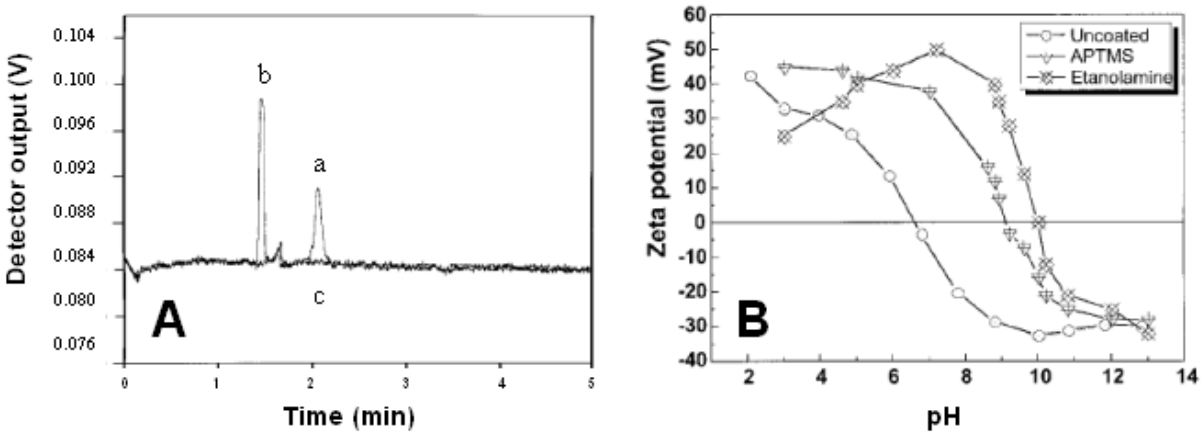


Figure 8. (A) Separation of the $Fe_3O_4$ nanoparticles (peak a) and the neutral marker mesityl oxide (peak b) by CE/UV at the wavelength of 200 nm. Curve (c) is the background electrolyte. (B) Microelectrophoretic measurements (ξ-potential) of the $Fe_3O_4$ nanoparticles (uncoated; APTM-aminopropyltrimethoxysilane-coated; ethanolamine-coated) in buffer solutions at different pH values.

### 4.1.2 Surface modification and bioconjugation of SPIONs

***Surface modification***: The surface modification of SPIONs with starch, ethanolamine or aminopropyltrimethoxysilane can be achieved by controlled co-precipitation of the particles in matrix of polymeric starch, ethanolamine or aminopropyltrimethoxysilane respectively. Gold coated MIONs were synthesized in a water-in-oil reverse microemulsion ($\mu E$) system by coprecipitation of magnetite and subsequent reduction of gold on the surface of the magnetite using $NaBH_4$.

***Bioconjugation***: To make SPIONs target specific, after modification, various biological substances such as antibodies, proteins, or targeting ligands can be conjugated to the particles. The bioconjugation most often occurs via covalent binding of the molecules to an active surface of the nanoparticle using bifunctional cross-linkers and methods of bioconjugation chemistry. In this experiment, ethanolamine or aminopropyltrimethoxysilane coated SPIONs with carboxylic or aminopropyltrimethoxysilane groups at their surface were conjugated to the model protein BSA using EDC as a zero-length cross-linker. The conjugation efficiency was estimated by CE/LIF.

### 4.1.3 Effects of surface modifications on MR image

To compare the contrast effects of Au-MIONs and Dextran-MIONs on MRI, the particles were tested by MRI in aqueous colloidal suspension. A dose-dependent attenuation of MRI signal intensities was observed in both types of particle. Au-MIONs showed a clear suppression of $T_2$-weighted spin echo signals by 16.2 % of the medium carrier (water) levels already at concentration of 0.001 μg Fe/μl, whereas Dextran-MIONs induced a similar effect (13.3% attenuation) firstly at the concentration of 0.01 μg Fe/μl. Accordingly, at 0.03 μg Fe/μl levels, Au-MIONs caused an almost complete attenuation in MRI signal intensity, whereas Dextran-MIONs still permitted 34.6% of $T_2$-weighted signals originating from the medium carrier (water). Au-MIONs were shown to exert powerful contrast-enhancing properties in MRI. A possible mechanism could be that the golden shell of the Au-MIONs might have further attributed to the $T_2$ relaxation by a possible disturbance of the local magnetic field caused by electromagnetic interaction with the applied excitation pulse during excitation.

## 4.2 Determination of bioconjugation efficiency of SPIONs using CE/LIF (*Paper II*)

NDA has no intrinsic fluorescence but in the presence of nucleophile (thiol, cyanide), it reacts with primary amines to form highly fluorescent derivatives (101-104). The electropherogram (Figure 9A) shows the peak of SPIONs-BSA-NDA conjugate eluting at 3.15 min, which was completely diminished in a sample from the magneto-extracted supernatant. The electropherogram of a standard solution of BSA (4 μg/ml) shows the peak of the BSA-NDA derivative eluting at 3.32 min. This demonstrates that the final sample of the bioconjugated nanoparticles contained BSA only in the form of SPIONs-BSA conjugates, since there was no detectable free BSA in the final carrier medium. In addition, the signal in the sample of the nanoparticle-BSA conjugates reflects the amount of the conjugated protein. The SPIONs in their `naked´ form, i.e. those not conjugated to the protein, could not react with the NDA reagent and resulted only in the same electropherogram as the blank sample. In addition, the `naked´ and non-derivatized nanoparticles did not produce any signal when injected into the CE/LIF system (Figure 9A).

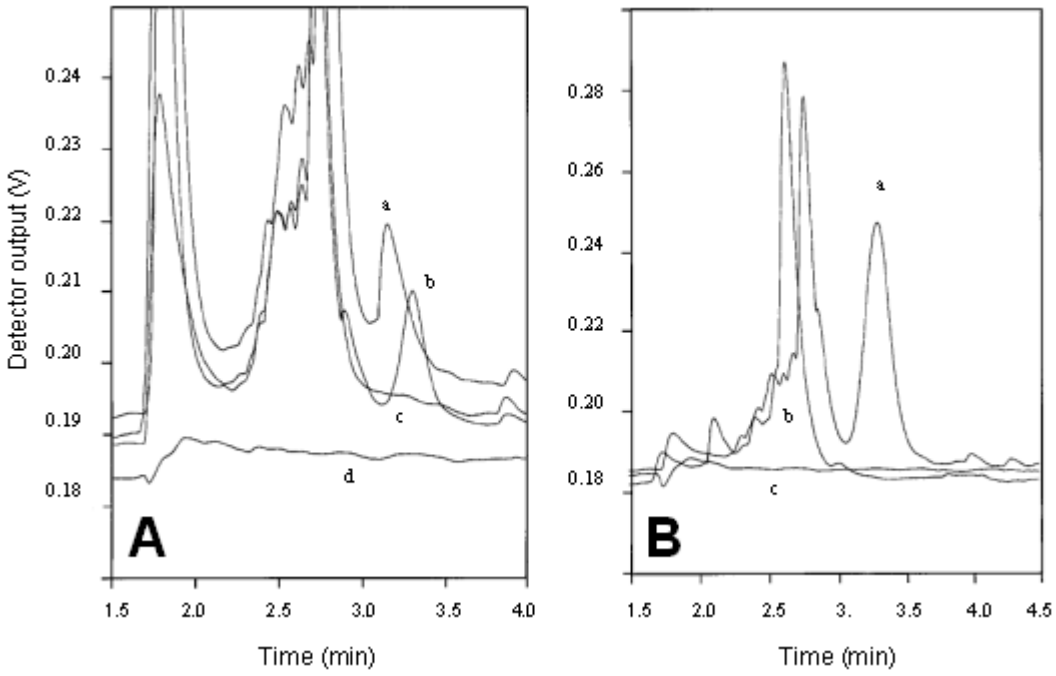


Figure 9. The electropherograms illustrating the separation and detection of functionalized iron oxide nanoparticles by CE/LIF following their derivatization with NDA. (A) Represents the $Fe_3O_4$-BSA-NDA conjugate (curve a), a standard solution of BSA-NDA derivative (curve b), the $Fe_3O_4$-NDA nanoparticles in their `naked´form, i.e. those not conjugated to the protein (curve c) and the `naked´and non-derivatized nanoparticles (curve d). (B) Represents the NDA-derivatized goat anti-rabbit IgG-coated MACS beads (curve a), the `naked´(no antibody) MACS beads (curve b) and the IgG-MACS particles not derivatized with NDA (curve c).

To test the ability of CE/LIF for determination of bioconjugated SPIONs with antibodies, the commercially available immunolabelled superparamagnetic iron oxide particles (MACS) were used. These particles are routinely used for magnetic cell sorting in cytochemistry. The electopherogram (Figure 9B) shows the detection of NDA-derivatized goat anti-rabbit immunoglobulin G (IgG)-coated MACS beads, whereas the peak of antibody was completely missing when the `naked´MACS beads were derivatized. When the IgG-beads were not derivatied with NDA, they did not produce any significant fluorescence signal (Figure 9B).

To test the ability of CE/LIF for determination of a direct conjugation of the fluorophore to the bioconjugated SPIONs, the recently introduced strong fluorescent Alexa Fluor$^{TM}$ 430 was conjugated via its succinimidyl ester moiety to the amino groups of the aminopropyltrimethoxysilanized nanoparticles. The Alexa-nonoparticle derivatives and that of Alexa itself gave signals in the electropherograms, which shows that the CE/LIF method

can also be used in combination with other derivatization reagents and chemistries for the characterization of protein-coupling efficiency to the iron oxide nanoparticles.

## 4.3 Surface modified SPIONs *in vivo* (*Paper III, IV, V*)

### 4.3.1 Diffusion and clearance of SPIONs in the rat striatum

***Starch-MIONs*:** To confirm the intensity of the transport/diffusion of Starch-MIONs through the extracellular space in the brain, Starch-MIONs were infused into the rat striatum and MRI was performed. On $T_2$* images, the MR signal intensity strongly reduced (black) and gradually from the center of the infusion toward the periphery, indicating that Starch-MIONs can diffuse through the extracellular space in rat brain.

***Dextran-MIONs*:** Dextran-MIONs were stereotaxically infused into the striatum of the anesthetized rats. MRI followed by histochemical staining of the Fe ions were performed at time intervals of 1, 3, 6, 12, 24, 48, 72 hours and 2 weeks after inoculation. The particles were infused at doses of 0.01; 0.1; 1 and 5 μg Fe/0.5 μl/min and at varying volumes (0.5, 3 and 9 μl). There was a good correlation between the MR signals and histochemical Fe staining at the reasonable doses. Both methods were capable of detecting as low as 0.1 μg Fe/0.5 μl, 1 hour postinjection, whereas the lowest dose of 0.01 μg Fe was not detectable. Infusion of 1 or 5 μg Fe/0.5 μl caused a dramatic increase of the labeled area 1 hour (5 μg Fe) or 24 hours (1 μg Fe) after inoculation, and similar effects were observed when increasing the volume of infused Fe. Two weeks after inoculation, the Fe signals were undetectable at 0.1 μg Fe and strongly attenuated at 1 and 5 μg Fe in MR image. Dextran-MIONs with their biocompatible surface coating can diffuse through the interstitial space of the brain and are progressively cleared out from the infusion site of the brain. The Dextran-MIONs can be beneficially used in MRI-guided diagnostic applications, or as labels and carriers for targeted drug delivery in the central nervous system.

***Au-MIONs*:** We speculate that since Au-MIONs expose their bare gold surfaces, they might anchor themselves to the surrounding tissue via chemisorb spontaneously to the substrates through the sulfur group, and because of its inert property, the Au shell might protect dissolution of Au-MIONs from the low pH environment of the lysosome (105, 106). If this is

true, Au-MIONs might have relatively long-term MRI contrast-enhancing properties in their target area *in vivo*. To prove this hypothesis, we infused Au-MIONs into the rat striatum at the doses of 0.1 or 1 μg Fe/0.5 μl, Dextron-MIONs were used as a control. MRI observed that the labeled area of Dextran-MIONs increased within increasing time in the brain, however Au- MIONs were static at the local injection area, no diffusion was observed. Two weeks later, the signals of the particles were obviously attenuated for Dextran-MIONs, whereas Au-MIONs still produced strong signals for both doses of 0.1 or 1 μg Fe/0.5 μl. Similar findings were found with the histological staining. These results provide preliminary evidence to support our hypothesis.

### 4.3.2 Evaluation of toxicity

The degree of tissue trauma caused by the infusion of Au-MIONs and Dextran-MIONs was evaluated by immunocytochemical staining of markers of dopaminergic neurons (TH), astrocyte (GFAP, VIM), microglia (OX-42) and NOS activation. There were no differences in distribution of TH positive dopaminergic neurons and staining of NOS were observed between treated animals and control. In all brains, reactive astrocytes were found surrounding the needle tract and the site of injection with GFAP, VIM labeling, and no difference was observed between Au-MIONs and Dextran-MIONs. Similarly, there was no difference between animals with Au-MIONs and Dextran-MIONs for staining of microglia (with OX-42), although both materials caused a slightly higher GFAP, VIM or OX-42 staining intensities than the control animals. Taken together, these results indicate that the biocompatility of Au-MIONs was similar with Dextran-MIONs.

## 4.4 NSCs labeling with Au-MIONs (*Paper IV, V*)

***Labeling efficiency of GDNF-NSCs with Au-MIONs***: Neonatal mouse cerebellum primary neural stem cell lines incubated with Au-MIONs or Dextran-MIONs for 24 hours. When these cells were incubated with Au-MIONs at the concentration of 10 μg Fe/ml, an efficacy of all of the cells were labelled for Au-MIONs was observed. However, no labeling was observed for the cell line incubated with Dextran-MIONs both at the concentration of 10 and 100 μg Fe/ml. In previous experiments, most nonphagocytic cells do not take up SPIONs efficiently which require cells to be exposed to high amounts of iron (2000 μg Fe/ml) in

culture (53, 55, 56), or in combination with a transfection agent (TA) (107, 108), but clinical application may be limited for TA using. The results of this study show that neuron stem cells can be labeled with low concentration of Au-MIONs (10 μg/ml) without TA. Since Au-MIONs expose their bare gold surfaces, they can chemisorb spontaneously to the substrates through the sulfur group. This would be one of the possibilities for them being attracted on the cells surface and stimulate phagocytosis.

***Labeling efficiency of GFP-NSCs with Au-MIONs*:** The GFP-NSCs in culture were identified by fluorescence microscopy of GFP expressed by the cells. Similarly, in immortalized cells, the silver enhancement histochemical protocol was used to examine the presence of gold-coated nanoparticles in the cell cytoplasm following 24 hours incubation. A good overlap between the GFP fluorescence and enhanced silver staining of gold nanoparticles was obtained. Interestingly, silver staining was restricted only to the cytosol and cell membrane indicating that Au-MIONs did not penetrate to the nucleus. Without the contrast agent, an 80% efficacy of cell labelling was obtained for Au-MIONs concentrations at 10 μg Fe/ml and 24 hours incubation period. Prolonged incubation to 48 hours or higher (20 μg Fe/ml) nanoparticle concentration had no enhancing effect on loading efficiency. The nanoparticle-labelled and control cells showed similar morphology and survival rate, with only 3% and 1.3% dead cells, respectively, estimated by trypan blue dye exclusion.

## 4.5 Tracking Au-MIONs labelled GFP-NSCs *in vivo* using MRI (*Paper V*)

***Detection limit of MRI for Au-MIONs labeled GFP-NSCs*:** To test the detection limit of MRI for Au-MIONs labeled GFP-NSCs, the suspensions of Au-MIONs labeled GFP-NSCs were injected into a 0.3% agar medium with different concentrations. MRI revealed that as few as 20 labelled cells resulted in 7.1% attenuation of $T_2$-weighted signals, while 200 labelled cells caused 21.6% attenuation compared to 200 non-labelled cells.

***Ttracking Au-MIONs labeled GFP-NSCs in the rat spinal cord***: The Au-MIONs labelled GFP-NSCs were infused into the rat spinal cord with a concentration of 1334 cells/μl. MRI was performed at 1 hour, 48 hours and 1 month after infusion. The labelled cells were

confined at the grafted site as a distinct dark area. No notable migration from the original site of infusion was observed during the study period.

***Histological conformation***: The MRI findings were closely correlated to those obtained by histological staining of Au-MIONs (silver enhancement) and GFP immunoreactivity for GFP-NSCs. However, several silver-stained cells were also immunopositive for ED1 staining, indicating that Au-MIONs from died stem cells were transferred to microglia and macrophages. These results suggest that the grafted cells do not migrate efficiently when implanted in the intact rat spinal cord. However, very few cells appeared to have survived to the one month time point, as revealed from the staining for GFP immunoreactivity, making it difficult to draw conclusions regarding the cell migration. One possible explanation is that the surviving cells could downregulate the GFP expression (109). In agreement with previous data on the stem cell survival in the host tissue (45), the occurrence of a number of ED1-positive reactive microglial cells at the site of implantation suggests that a substantial number of stem cells have died one month after the transplantation. This is also reflected by the overlap between the histochemical staining of the Au-MIONs and the immunohistochemical staining of the microglia.

# 5 CONCLUSIONS

SPIONs can be functionalized with proteins, antibodies or other primary amino group containing molecules. The coating efficiency can be monitored by CE/LIF. Both Starch-MIONs and Dextran-MIONs were capable of diffusing through the interstitial space of brain parenchyma, which can be beneficially used in drug or molecule target delivery and MRI applications for tracing and therapy. Au-MIONs possess superior stability and surface properties, the latter enabling rapid cellular uptake of the particles already at physiological conditions. These properties make Au-MIONs especially suitable for tracking of transplated cells by MRI.

# 6 ACKNOWLEDGEMENTS

This study was carried out at the Department of Clinical Neuroscience and the Department of Neuroscience, the theoretical part was finalized at the Department of Physiology and Pharmacology, Karolinska Institutet, Stockholm, Sweden. I would like to express my sincere gratitude to all the people who have helped me through these years and contributed to make this thesis possible, especially to:

Dr. Jan Kehr, my supervisor, for giving me the opportunity to make my Ph.D. degree in Karolinska Institutet, for introducing me into the field of Applications of Magnetic Nanoparticles in Biomedicine, for scientific guidance and for his support and help in the past years.

Professor Börje Bjelke, my co-supervisor, for his never failing and invaluable support, for scientific guidance and discussions with his profound scientific knowledge and scientific ethics, for helping me to scrutinize the manuscripts.

Professor Sven Ove Ögren, my co-supervisor, for giving me the opportunity to work at his lab with an excellent scientific working atmosphere, for his support and encouragement during these years.

Professor Christian Spenger, my co-supervisor, for his support, and great interest in my work and for inspiring scientific discussions.

All the former and present members in the group, especially:
Ms. Paula Mannström, Ms. Karin Snitt and Ms. Anette Fransson, for help in the lab; Dr. Pär A. Schött, Dr. Haleh Razani, Dr. Johan Sandin, Dr. Takashi Yoshitake, Ms. Shimako Yoshitake, Dr. Alexander Kuzmin, Dr. Peter Osborne, Dr. Ilga Misane, Dr. Lydia Gimenez-Liort, Dr. Maria Lűttgen, Dr. Elin Elvander, Dr. Nather Madjid, Tottie, Dr. Eugenia Kuteeva, Dr. Sarah Holst, and Dr. Wardi Tara for support and interest.

Personnel of the MR Center at Karolinska Institutet:

Dr. Toms Klason for introducing me to the world of MRI; Dr. Xingchen Wu and Dr. Johan Lilja for help and support.
The Department of Neuroscience:
Professor Kjell Fuxe, Professor Lars Olson, Professor Thomas Hökfelt, Professor Björn Meistar, for their support; Dr. I-Hui Lee, for excellent collaboration in stem cells labeling with magnetic nanoparticles; Dr. Saga Johansson, for her commendable collaboration in evaluation of nanoparticles´ toxicity in rat model; Ms. Anne Edgren, Dr. Malin Hoistad, Ms. Ida Engqvist, Dr. Zhi-Qing David Xu, Dr. Tie-Jun Shi, Dr. Wei Zhang, Dr. Yuxuan Jin, Dr. Yong Liang and Dr. Hu Hu for friendship.

The Department of Physiology and Pharmacology:
Professor Stefan Eriksson, the head of the department, for his invaluable support; Associate Professor Inger Johansson, Professor Ernst Brodin, for improving my knowledge in pharmacology; Ms. Louise Bovin, for her deep support; Professor Urban Ungerstedt and Dr. Michel Goiny for friendship.

The Department of Medical Biochemistry and Biophysics:
Dr. Carmen Saltó and Professor Ernest Arenas, for their collaboration in stem cells labeling with magnetic nanoparticles.

The Department of Cell and Molecular Biology:
Dr. Niklas Holmström and Professor Jonas Frisén, for collaboration in stem cells labeling with magnetic nanoparticles.

The Department of Materials Science, Royal Institute of Technology, Stockholm, Sweden:
Dr. Do Kyung Kim, Dr. Maria Mikhaylova and Professor Mamoun Muhammed, for their excellent collaboration in magnetic nanoparticles.

Fellow colleagues at AstraZeneca:
Dr. Susanne Fabre, for her invaluable support; Mr. Andres Andersson, Dr. Mattias Lindberg, Dr. Jeremy Young and Ms. Camilla Jacobsson, for support and friendship, especially, Dr. Tomas Klason, for discussions about MRI.

Friends outside the Departments:
Dr Ping-Sheng Hu and Mr. Mikael Wrong, for being kindly helpful; Dr. Andrew Turnbull, for improving my English writing; Dr. Lei Wei, Dr. Xiao-Juan Sun and Dr. Jun Zhou, for the friendship; Especially, Mr. Yu Jiang, my old friend, for his support encouragement.

I have to mention my former supervisor, Professor Du-Li Tang. He introduced me to the medical science. I am greatly impressed by his outstanding personality and deep knowledge, especially in the field of general surgery.

Professor Curt Einarsson, for inviting me to come to Sweden as a visiting scientist in his lab, for introducing me into the excellent Swedish scientific atmosphere.

I am indebted to Xiao-Qiu, Bo Ding, Lan-Lan, Joakim and Xue-er, for their support and making my life pleasant.

I would like to thank my elder brother, Jian-Hua, my three elder sisters and brothers-in-law, especially, Jin-Li, for persistent support and encouragement. Without your help, this would not have been possible.

I would also like to thank my mother-in-law Xiang Lu, sisters-in-law and younger brother-in-law, for support and understanding.

Xiao-Jing, my beloved wife, for all your support and encouragement, for sharing all my happiness and sorrows. Without your help and understanding, this would have been impossible.

My son, Peng-Chun, he was a little boy when he came to Sweden with us, I have watched him grow up, for bringing me a troublesome but really enjoyable life. Now, he is a university student. I would like to thank him for love, support and the help in improving my English.

These studies were supported by the grants from the Swedish Foundation for Strategic Research, International Cooperation in Research and Higher Education, STINT (T.Y.).

# 7 REFERENCE


1. Vré RMD, Lemort M. (1995) Biophysical properties and clinical applications of magnetic resonance imaging contrast agents. *British Journal of Radiology* **68:** 225-247.

2. Hofmann H, Petri-Fink A, Steitz B, Rechenberg Bv, Hofmann M, Juillerat J. (2005) Superparamagnetic Iron Oxide Nanoparticles for Multiple Biomedical Applications. *Nanotechnology* **1:** 152 - 155.

3. Kim EH, Ahn Y, Lee HS. (2006) Biomedical applications of superparamagnetic iron oxide nanoparticles encapsulated within chitosan. *Journal of Alloys and Compounds* **434-435:** 633-636.

4. Cengelli F, Tschudi-Monnet F, Maysinger D, et al. (2007) SuperParamagnetic Iron Oxide Nanoparticles: a multifunctional tool in biomedical applications. *European Cells and Materials* **13:** 12.

5. Lin MM, Kim do K, El Haj AJ, Dobson J. (2008) Development of superparamagnetic iron oxide nanoparticles (SPIONS) for translation to clinical applications. *IEEE Trans Nanobioscience* **7:** 298-305.

6. Schellenberger E. (2009) Bioresponsive nanosensors in medical imaging. *J R Soc Interface* **7 Suppl 1:** S83-91.

7. Nabeshima M, Moriyasu F, Ono S, et al. (1993) Selective MR angiography of the liver. *J Comput Assist Tomogr* **17:** 730-734.

8. Poon I, Fischbein N, Lee N, et al. (2004) A population-based atlas and clinical target volume for the head-and-neck lymph nodes. *Int J Radiat Oncol Biol Phys* **59:** 1301-1311.

9. Rose J, Butler EE, Lamont LE, Barnes PD, Atlas SW, Stevenson DK. (2009) Neonatal brain structure on MRI and diffusion tensor imaging, sex, and neurodevelopment in very-low-birthweight preterm children. *Dev Med Child Neurol* **51:** 526-535.

10. Freiman M, Edrei Y, Sela Y, et al. (2008) Classification of suspected liver metastases using fMRI images: a machine learning approach. *Med Image Comput Comput Assist Interv* **11:** 93-100.

11. Kay KN, Naselaris T, Prenger RJ, Gallant JL. (2008) Identifying natural images from human brain activity. *Nature* **452:** 352-355.

12. Stroman PW. (2009) Spinal fMRI investigation of human spinal cord function over a range of innocuous thermal sensory stimuli and study-related emotional influences. *Magn Reson Imaging* **27:** 1333-1346.

13. Brähler M, Georgieva R, Buske N, et al. (2006) Magnetite-Loaded Carrier Erythrocytes as Contrast Agents for Magnetic Resonance Imaging. *Nano Letters* **6:** 2505–2509.

14. Barrett T, Brechbiel M, Bernardo M, Choyke PL. (2007) MRI of tumor angiogenesis. *J Magn Reson Imaging* **26:** 235-249.

15. Branca R, Clevelandb Z, Fubarab B, et al. (2010) Molecular MRI for sensitive and specific detection of lung metastases. *PNAS* **107:** 3693-3697.

16. Sun C, Veiseh O, Gunn J, et al. (2008) In vivo MRI detection of gliomas by chlorotoxin-conjugated superparamagnetic nanoprobes. *Small* **4:** 372-379.

17. Yang X, Pilla S, Grailer J, et al. (2009) Tumor-targeting, superparamagnetic polymeric vesicles as highly efficient MRI contrast probes. *Journal of Materials Chemistry* **19:** 5812 - 5817.

18. To SY, Castro DJ, Lufkin RB, Soudant J, Saxton RE. (1992) Monoclonal antibody-coated magnetite particles as contrast agents for MR imaging and laser therapy of human tumors. *J Clin Laser Med Surg* **10:** 159-169.

19. Alexiou C, Arnold W, Klein RJ, et al. (2000) Locoregional cancer treatment with magnetic drug targeting. *Cancer Res* **60:** 6641-6648.

20. Rudge SR, Kurtz TL, Vessely CR, Catterall LG, Williamson DL. (2000) Preparation, characterization, and performance of magnetic iron-carbon composite microparticles for chemotherapy. *Biomaterials* **21:** 1411-1420.

21. Lin MM, Kim HH, Kim H, Dobson J, Kim do K. (2010) Surface activation and targeting strategies of superparamagnetic iron oxide nanoparticles in cancer-oriented diagnosis and therapy. *Nanomedicine (Lond)* **5:** 109-133.

22. Gupta AK, Gupta M. (2005) Synthesis and surface engineering of iron oxide nanoparticles for biomedical applications. *Biomaterials* **26:** 3995-4021.

23. Laurent S, Forge D, Port M, et al. (2008) Magnetic iron oxide nanoparticles: synthesis, stabilization, vectorization, physicochemical characterizations, and biological applications. *Chem Rev* **108:** 2064-2110.

24. Hofmann-Amtenbrink M, von Rechenberg B, Hofmann H. (2009) Superparamagnetic nanoparticles for biomedical applications. In: Tan MC (ed.). Transworld Research Network, Kerala, India, pp. 119-149.

25. Bartolozzi C, Lencioni R, Donati F, Cioni D. (1999) Abdominal MR: liver and pancreas. *Eur Radiol* **9:** 1496-1512.

26. Dousset V, Gomez C, Petry KG, Delalande C, Caille JM. (1999) Dose and scanning delay using USPIO for central nervous system macrophage imaging. *Magma* **8:** 185-189.

27. Ros PR, Freeny PC, Harms SE, et al. (1995) Hepatic MR imaging with ferumoxides: a multicenter clinical trial of the safety and efficacy in the detection of focal hepatic lesions. *Radiology* **196:** 481-488.

28. Hamberg LM, Boccalini P, Stranjalis G, et al. (1996) Continuous assessment of relative cerebral blood volume in transient ischemia using steady state susceptibility-contrast MRI. *Magn Reson Med* **35:** 168-173.

29. Varallyay C, Leslie L Muldoon L, Gahramanov S, et al. (2009) Dynamic MRI using iron oxide nanoparticles to assess early vascular effects of antiangiogenic versus corticosteroid treatment in a glioma model. *J Cereb Blood Flow Metab* **29(4):** 853-860.

30. van Bruggen N, Busch E, Palmer JT, Williams SP, de Crespigny AJ. (1998) High-resolution functional magnetic resonance imaging of the rat brain: mapping changes in cerebral blood volume using iron oxide contrast media. *J Cereb Blood Flow Metab* **18:** 1178-1183.

31. Goense JBM, Zappe A-C, Logothetis HK. (2007) High-resolution fMRI of macaque V1. *Magnetic Resonance Imaging* **25(6):** 740-747.

32. Janssens T, Vanduffel W, Kolster H. (2009) SNR Optimization of MION fMRI in the anaesthetized monkey using an 8-channel PA-coil and accelerated imaging. *Proc. Intl. Soc. Mag. Reson. Med.* **17:** 1619.

33. Ichikawa T, Arbab AS, Araki T, et al. (1999) Perfusion MR imaging with a superparamagnetic iron oxide using T2-weighted and susceptibility-sensitive echoplanar sequences: evaluation of tumor vascularity in hepatocellular carcinoma. *AJR Am J Roentgenol* **173:** 207-213.

34. Pathak AP. (2009) Magnetic resonance susceptibility based perfusion imaging of tumors using iron oxide nanoparticles. *Wiley Interdiscip Rev Nanomed Nanobiotechnol* **1:** 84-97.

35. Weissleder R, Lee AS, Khaw BA, Shen T, Brady TJ. (1992) Antimyosin-labeled monocrystalline iron oxide allows detection of myocardial infarct: MR antibody imaging. *Radiology* **182:** 381-385.

36. VARALLYAY C, G, MULDOON L, L. , GAHRAMANOV S, et al. (2009) Dynamic MRI using iron oxide nanoparticles to assess early vascular effects of antiangiogenic versus corticosteroid treatment in a glioma model. *Journal of cerebral blood flow and metabolism* **29:** 853-860.

37. Weissleder R, Lee AS, Fischman AJ, et al. (1991) Polyclonal human immunoglobulin G labeled with polymeric iron oxide: antibody MR imaging. *Radiology* **181:** 245-249.

38. Sosnovik DE, Weissleder R. (2007) Emerging concepts in molecular MRI. *Current Opinion in Biotechnology* **18:** 4-10.

39. Xie J, Chen K, Lee HY, et al. (2008) Ultrasmall c(RGDyK)-coated Fe3O4 nanoparticles and their specific targeting to integrin alpha(v)beta3-rich tumor cells. *J Am Chem Soc* **130:** 7542-7543.

40. Corot C, Robert P, Idee JM, Port M. (2006) Recent advances in iron oxide nanocrystal technology for medical imaging. *Adv Drug Deliv Rev* **58:** 1471-1504.

41. Solanki A, John D Kim JD, Lee KB. (2008) Nanomaterials for Stem Cell Imaging: Magnetic Nanomaterials: Iron Oxide Nanoparticles. *Nanomedicine (Lond)* **3(4):** 567-578.

42. Budde MD, Frank JA. (2009) Magnetic tagging of therapeutic cells for MRI. *J Nucl Med* **50:** 171-174.

43. Yeh TC, Zhang W, Ildstad ST, Ho C. (1995) In vivo dynamic MRI tracking of rat T-cells labeled with superparamagnetic iron-oxide particles. *Magn Reson Med* **33:** 200-208.

44. Krieg FM, Andres RY, Winterhalter KH. (1995) Superparamagnetically labelled neutrophils as potential abscess-specific contrast agent for MRI. *Magn Reson Imaging* **13:** 393-400.

45. Lee IH, Bulte JW, Schweinhardt P, et al. (2004) In vivo magnetic resonance tracking of olfactory ensheathing glia grafted into the rat spinal cord. *Exp Neurol* **187:** 509-516.

46. Handgretinger R, Lang P, Schumm M, et al. (1998) Isolation and transplantation of autologous peripheral CD34+ progenitor cells highly purified by magnetic-activated cell sorting. *Bone Marrow Transplant* **21:** 987-993.

47. Gupta AK, Curtis AS. (2004) Lactoferrin and ceruloplasmin derivatized superparamagnetic iron oxide nanoparticles for targeting cell surface receptors. *Biomaterials* **25:** 3029-3040.

48. Janic B, Rad AM, Jordan EK, et al. (2009) Optimization and validation of FePro cell labeling method. *PLoS One* **4:** e5873.

49. Schoepf U, Marecos EM, Melder RJ, Jain RK, Weissleder R. (1998) Intracellular magnetic labeling of lymphocytes for in vivo trafficking studies. *Biotechniques* **24:** 642-646, 648-651.

50. Kalambur VS, Longmire EK, Bischof JC. (2007) Cellular level loading and heating of superparamagnetic iron oxide nanoparticles. *Langmuir* **23:** 12329-12336.

51. Cuatrecasas P, Roth T. (1983) Receptor-mediated endocytosis. Kluwer Academic Publishers, Dordrecht.

52. Ahrens ET, Feili-Hariri M, Xu H, Genove G, Morel PA. (2003) Receptor-mediated endocytosis of iron-oxide particles provides efficient labeling of dendritic cells for in vivo MR imaging. *Magn Reson Med* **49:** 1006-1013.

53. Weissleder R, Cheng HC, Bogdanova A, Bogdanov A, Jr. (1997) Magnetically labeled cells can be detected by MR imaging. *J Magn Reson Imaging* **7:** 258-263.

54. Bouzier-Sore AK, Ribot E, Bouchaud V, et al. (2010) Nanoparticle phagocytosis and cellular stress: involvement in cellular imaging and in gene therapy against glioma. *NMR Biomed* **23:** 88-96.

55. Bulte JW, Laughlin PG, Jordan EK, Tran VA, Vymazal J, Frank JA. (1996) Tagging of T cells with superparamagnetic iron oxide: uptake kinetics and relaxometry. *Acad Radiol* **3 Suppl 2:** S301-303.

56. Dodd SJ, Williams M, Suhan JP, Williams DS, Koretsky AP, Ho C. (1999) Detection of single mammalian cells by high-resolution magnetic resonance imaging. *Biophys J* **76:** 103-109.

57. Josephson L, Groman EV, Menz E, Lewis JM, Bengele H. (1990) A functionalized superparamagnetic iron oxide colloid as a receptor directed MR contrast agent. *Magn Reson Imaging* **8:** 637-646.

58. Alexiou C, Schmid RJ, Jurgons R, et al. (2006) Targeting cancer cells: magnetic nanoparticles as drug carriers. *Eur Biophys J* **35:** 446-450.

59. Yuan Q, Venkatasubramanian R, Hein S, Misra RD. (2008) A stimulus-responsive magnetic nanoparticle drug carrier: magnetite encapsulated by chitosan-grafted-copolymer. *Acta Biomater* **4:** 1024-1037.

60. Chouly C, Pouliquen D, Lucet I, Jeune JJ, Jallet P. (1996) Development of superparamagnetic nanoparticles for MRI: effect of particle size, charge and surface nature on biodistribution. *J Microencapsul* **13:** 245-255.

61. Gupta AK, Wells S. (2004) Surface-modified superparamagnetic nanoparticles for drug delivery: preparation, characterization, and cytotoxicity studies. *IEEE Trans Nanobioscience* **3:** 66-73.

62. Wu W, He Q, Jiang C. (2008) Magnetic Iron Oxide Nanoparticles: Synthesis and Surface Functionalization Strategies. *Nanoscale Research Letters* **3:** 397-415.

63. Kresse M, Wagner S, Pfefferer D, Lawaczeck R, Elste V, Semmler W. (1998) Targeting of ultrasmall superparamagnetic iron oxide (USPIO) particles to tumor cells in vivo by using transferrin receptor pathways. *Magn Reson Med* **40:** 236-242.

64. Pratsinis S, Vemury S. (1996) Particle formation in gases-a review. *Powder Technol* **188:** 267.

65. Kamau SW, Schulze K, Steitz B, et al. (2005) Superparamagnetic iron oxide nanoparticle (SPIONs) as non-viral vectors for gene delivery in vitro. *European Cells and Materials* **10:** 10.

66. Kamau SW, Hassa PO, Steitz B, et al. (2006) Enhancement of the efficiency of non-viral gene delivery by application of pulsed magnetic field. *Nucleic Acids Res* **34:** e40.

67. Nielsen OS, Horsman M, Overgaard J. (2001) A future for hyperthermia in cancer treatment? *Eur J Cancer* **37:** 1587-1589.

68. Ito A, Shinkai M, Honda H, Kobayashi T. (2005) Medical application of functionalized magnetic nanoparticles. *J Biosci Bioeng* **100:** 1-11.

69. Short JG, Turner PF. (1980) Physical hyperthermia and cancer therapy. *Proceedings of the IEEE* **68:** 133-142.

70. Luderer AA, Borrelli NF, Panzarino JN, et al. (1983) Glass-ceramic-mediated, magnetic-field-induced localized hyperthermia: response of a murine mammary carcinoma. *Radiat Res* **94:** 190-198.

71. Jordan A, Scholz R, Wust P, Schirra H. (1999) Endocytosis of dextran and silan-coated magnetite nanoparticles and the effect of intracellular hyperthermia on human mammary carcinoma cells in vitro. *J. Magn. Magn. Mater.* **194:** 185-196.

72. Sneed P, Stea B. (1996) Thermoradiotherapy and thermochemotherapy. Springer, Berlin.

73. Hildebrandt B, Rau B, Gellermann J, Wust P, Riess H. (2004) Hyperthermic intraperitoneal chemotherapy in patients with peritoneal carcinosis. *J Clin Oncol* **22:** 1527-1529; author reply 1529.

74. Lu AH, Salabas EL, Schüth F. (2007) Magnetic Nanoparticles: Synthesis, Protection, Functionalization, and Application. *Angewandte Chemie International Edition* **46:** 1222 - 1244.

75. Marco MD, Sadun C, Port M, Guilbert I, Couvreur P, Dubernet C. (2007) Physicochemical characterization of ultrasmall superparamagnetic iron oxide particles (USPIO) for biomedical application as MRI contrast agents. *Int J Nanomedicine* **2(4):** 609–622.

76. Portet D, Denizot B, Rump E, Lejeune JJ, Jallet P. (2001) Nonpolymeric Coatings of Iron Oxide Colloids for Biological Use as Magnetic Resonance Imaging Contrast Agents. *J Colloid Interface Sci* **238:** 37-42.

77. Sahoo Y, Goodarzi A, Swihart MT, et al. (2005) Aqueous ferrofluid of magnetite nanoparticles: Fluorescence labeling and magnetophoretic control. *J Phys Chem B* **109:** 3879-3885.

78. Lacava LM, Lacava ZG, Da Silva MF, et al. (2001) Magnetic resonance of a dextran-coated magnetic fluid intravenously administered in mice. *Biophys J* **80:** 2483-2486.

79. Zhang Y, Kohler N, Zhang M. (2002) Surface modification of superparamagnetic magnetite nanoparticles and their intracellular uptake. *Biomaterials* **23:** 1553-1561.

80. Wang Q, Su H, Xia C, et al. (2009) Amphiphilic dextran/magnetite nanocomposites as magnetic resonance imaging probes. *Chinese Sci Bull* **54:** 2925-2933.

81. Del campo A, Sen T, Lellouche L, Bruce I. (2005) Multifunction magnetitie and silica-magnetite nanoparticles: synthesis, surface activation and applications in lift sciences. *Journal of Magnetism and Magnetic Materials* **293:** 33-40.

82. Kim J, Park S, Lee J, et al. (2006) Designed fabrication of multifunctional magnetic gold nanoshells and their application to magnetic resonance imaging and photothermal therapy. *Angewandte Chemie. International edition in English* **45:** 7754-7758.

83. Roberts MJ, Bentley MD, Harris JM. (2002) Chemistry for peptide and protein PEGylation. *Adv Drug Deliv Rev* **54:** 459-476.

84. Xie J, Xu C, Kohler N, Hou Y, Sun S. (2007) Controlled PEGylation of monodisperse Fe3O4 nanoparticles for reduced non-specific uptake by macrophage cells. *Advanced Materials* **19:** 3163-3166.

85. Sitharaman B, Wilson LJ. (2006) Gadonanotubes as new high-performance MRI contrast agents. *Int J Nanomedicine* **1(3):** 291–295.

86. Wang YX, Hussain SM, Krestin GP. (2001) Superparamagnetic iron oxide contrast agents: physicochemical characteristics and applications in MR imaging. *Eur Radiol* **11:** 2319-2331.

87. Shen T, Weissleder R, Papisov M, Brady T. (1991) Polymeric iron oxide compounds for MR imaging *10th Annual Meeting of the Society of Magnetic Resonance in Medicine*, San Francisco, CA, p. 870.

88. Shen T, Weissleder R, Papisov M, Bogdanov A, Jr., Brady TJ. (1993) Monocrystalline iron oxide nanocompounds (MION): physicochemical properties. *Magn Reson Med* **29:** 599-604.

89. Kim D, Zhang Y, Kehr J, Klason T, Bjelke B, Muhammed M. (2001) Characterization and MRI study of surfactant-coated superparamagnetic nanoparticles administered into the rat brain. *Journal of Magnetism and Magnetic Materials* **225:** 256-261.

90. Kim D, Voit W, Zapka W, Bjelke B, Muhammed M, Rao K. (2001) synthesis and characterization of surfactant-coated superparamagnetic monodispersed iron oxide nanoparticles. *Journal of Magnetism and Magnetic Materials* **225:** 30-36.

91. Kim D, Mikhaylova M, Torpak M, et al. (2002) In-situ gold coating of superparamagnetic nanoparticles by microemulsion method. *Materials Research Society* **704:** 1-6.

92. Akerud P, Canals JM, Snyder EY, Arenas E. (2001) Neuroprotection through delivery of glial cell line-derived neurotrophic factor by neural stem cells in a mouse model of Parkinson's disease. *J Neurosci* **21:** 8108-8118.

93. Akerud P, Holm PC, Castelo-Branco G, Sousa K, Rodriguez FJ, Arenas E. (2002) Persephin-overexpressing neural stem cells regulate the function of nigral

dopaminergic neurons and prevent their degeneration in a model of Parkinson's disease. *Mol Cell Neurosci* **21:** 205-222.

94. Johansson CB, Momma S, Clarke DL, Risling M, Lendahl U, Frisen J. (1999) Identification of a neural stem cell in the adult mammalian central nervous system. *Cell* **96:** 25-34.

95. Falk A, Holmstrom N, Carlen M, Cassidy R, Lundberg C, Frisen J. (2002) Gene delivery to adult neural stem cells. *Exp Cell Res* **279:** 34-39.

96. Hennig J, Nauerth A, Friedburg H. (1986) RARE imaging: a fast imaging method for clinical MR. *Magn Reson Med* **3:** 823-833.

97. Neuwelt EA, Weissleder R, Nilaver G, et al. (1994) Delivery of virus-sized iron oxide particles to rodent CNS neurons. *Neurosurgery* **34:** 777-784.

98. Jansson A, Tinner B, Steinbusch HW, Agnati LF, Fuxe K. (1998) On the relationship of 5-hydroxytryptamine neurons to 5-hydroxytryptamine 2A receptor-immunoreactive neuronal processes in the brain stem of rats. A double immunolabelling analysis. *Neuroreport* **9:** 2505-2511.

99. Baker D. (1995) Capillary electrophoresis. Wiley, New York.

100. Camilleri P. (1993) Capillary Electrophoresis. Theory and Practice, CRC Press, Boca Raton, FL.

101. Bert L, Robert F, Denoroy L, Renaud B. (1996) High-speed separation of subnanomolar concentrations of noradrenaline and dopamine using capillary zone electrophoresis with laser-induced fluorescence detection. *Electrophoresis* **17:** 523-525.

102. Bert L, Robert F, Denoroy L, Stoppini L, Renaud B. (1996) Enhanced temporal resolution for the microdialysis monitoring of catecholamines and excitatory amino acids using capillary electrophoresis with laser-induced fluorescence detection. Analytical developments and in vitro validations. *J Chromatogr A* **755:** 99-111.

103. Freed A, Lunte S. (2000) Separation of naphthalene-2,3-dicarboxaldehyde-derivatized-substance P and its metabolites by micellar electrokinetic chromatography. *Electrophoresis* **21:** 1992-1996.

104. Oates MD, Jorgenson JW. (1989) Determination of naphthalene-2,3-dicarboxaldehyde-labeled amino acids by open tubular liquid chromatography with electrochemical detection. *Anal Chem* **61:** 432-435.

105. Ohkuma S, Poole B. (1978) Fluorescence probe measurement of the intralysosomal pH in living cells and the perturbation of pH by various agents. *Proc Natl Acad Sci U S A* **75:** 3327-3331.

106. Kreyling WG. (1992) Intracellular particle dissolution in alveolar macrophages. *Environ Health Perspect* **97:** 121-126.

107. Kraitchman DL, Heldman AW, Atalar E, et al. (2003) In vivo magnetic resonance imaging of mesenchymal stem cells in myocardial infarction. *Circulation* **107:** 2290-2293.

108. Arbab AS, Yocum GT, Wilson LB, et al. (2004) Comparison of transfection agents in forming complexes with ferumoxides, cell labeling efficiency, and cellular viability. *Mol Imaging* **3:** 24-32.

109. Hofstetter CP, Holmstrom NA, Lilja JA, et al. (2005) Allodynia limits the usefulness of intraspinal neural stem cell grafts; directed differentiation improves outcome. *Nat Neurosci* **8:** 346-353.